

Binder burnout and sintering kinetic study of alumina ceramics shaped using methylcellulose

K. Rajeswari, S. Chaitanya, P. Biswas, M. Buchi Suresh, Y.S. Rao and Roy Johnson*

Center for Ceramic Processing, International Advanced Research Centre for Powder Metallurgy and New Materials (ARCI), Balapur, Hyderabad, AP, 500 005, India

Ceramic components are generally processed by the techniques such as compaction, extrusion, injection molding, casting etc., and the selection of forming method is generally based on the complexity of the shapes. Additives such as binders, plasticizers, surfactants and lubricants, which are generally organic in nature, play a significant role to ensure the flowability of the mass which is critical in shaping of ceramics. Alumina (α -Al₂O₃) powder was subjected to torque rheometric studies to identify Critical Volume Binder Concentrations (CBVC) corresponding to specific processing regimes. An initial torque value of 3-4N-m for compaction followed by 6-7N-m for extrusion and 2-3N-m for casting regimes were observed. Viscosities of the pre-mixes prepared by the addition of methyl cellulose (C₆H₇O₂ (OH)_x(OCH₃)_y, (where x = 1.0-1.5 and y = 2-1.45) as a binder were also found to exhibit a similar trend in viscosity, corresponding to CBVC torque values and are shaped into green specimens. Green strength of the standard specimens (45 × 4 × 3 mm) was estimated through 3-point bend tests and exhibited a good correlation with the binder content. Binder burnout characteristics were also elucidated by TG/DSC technique and activation energy estimated is 75-110 kJ/mol for the thermal degradation of methylcellulose binder. Activation energy of 883 ± 45 kJ/mol was estimated through kinetic analysis of sintering by the construction of the Master Sintering Curves (MSC).

Key words: CBVC, Alumina, Rheology, Flexural strength, Thermal degradation.

Introduction

Green properties of ceramic components are very much depend on the powder packing and the additives such as binders, plasticizers, dispersants, surfactants and lubricants plays a major role, irrespective of the various processing techniques [1-5]. These additives are added to the powders or powder dispersed in a medium which reduces the inter-particle friction strongly affecting the rheological properties of the mix thereby improving the flowability while forming [6-8]. However, removal of these additives is an important part of the ceramic processing and the strength of the green compact will decrease as the binder is removed with a simultaneous pressure build-up from gaseous products, resulting from binder degradation [9-12]. This will raise the gas pressure that exceeds the stress tolerance of the components and the defects will be introduced. In order to avoid these defects, air holes and cracks, it is important to select right organic additives and with optimum proportions [13-15].

Removal of wax binder from injection molded part is described in terms of three mechanisms such as binder loss due to melting and thermal expansion, wicking of liquid binder due to capillary pull from the setter bed

and binder volatilization [16]. Substantial optimization of binder removal schedules is necessary to eliminate the cracking especially for samples with large cross section. Some of the non-oxide ceramic systems, such as silicon carbide system may contain multi-component species which degrade during thermal decomposition to additional species. Thermal decomposition rate and generation rate of the new species play a major role in the controlled removal of the binder [17]. Methylcellulose is a versatile binder in ceramic processing composed of two components such as cellulose and methyl (-CH₃) side chains. Cellulose itself is water insoluble, long chain molecule consisting of repeating anhydrous glucose units. Cellulose with methyl substitution has very good compatibility characteristics with most of the common ceramic systems [18]. Methyl cellulose is widely used for extrusion and injection moulding as they undergo thermally induced gelation at temperatures in the range of 50-60 °C.

The present study is aimed on the exploration of methyl cellulose as a binder for a widely used ceramic alumina (α -Al₂O₃) powder employing three processing methodologies such as compaction, extrusion and casting. α -Al₂O₃ procured from a commercial source has been subjected to torque rheometric studies to identify the Binder Concentration corresponding to specific processing regimes. These regimes, such as sub CBVC (critical binder volume concentration), CBVC and post CBVC, corresponds to compaction, extrusion and casting. Mixes were prepared with

*Corresponding author:
Tel : +914024443169
Fax: +914024442699
E-mail: royjohnson@arci.res.in

varying concentrations of methyl cellulose suitable for compaction, extrusion and casting processes and the optimum concentration was identified through the maximum green strength. The green samples were also characterized for TG/DSC and the activation energy of the methylcellulose thermolysis was estimated. Samples were further sintered at 1600 °C to comparatively evaluate the final sintered densities under identical conditions.

Experimental Procedure

Processing regimes

Commercial alumina (HP grade), procured from ACC, Mumbai, India, was characterized for the powder properties such as particle size, surface area and were subjected to CBVC measurements. 60 gm of alumina was titrated against the linseed oil in a Brabender Rheometer PL 2000 mixer and the torque against the binder volume concentration was recorded. In this experiment, wetting liquid such as linseed oil (binder) is added in installments to the powder and the mixing torque is monitored as the mix is continuously sheared by means of a specially contoured rotating blades. Considering the volume of the oil added and the equilibrium torque value achieved after each addition, a plot is drawn with the ordinate representing the equilibrium torque values and the abscissa in terms of the percentage volume of binder in the mix. Based on the Binder Volume Concentration regimes, alumina mix were prepared with water and methyl cellulose as a binder. Binder requirements for the various regimes were estimated using green strength measurements and finally sintered under identical conditions.

Elucidation of flow behavior

Alumina granules corresponding to the sub-CBVC regime are prepared with 1 wt % of methyl cellulose and flow properties in terms of cohesion index were evaluated using a powder flow analyzer attached to a Texture Analyzer as per the procedure described elsewhere [19]. In order to measure powder flow characteristics, 50 g of granules were placed in a cylinder and a helical blade moves within the cylinder, which in turn comes the movement of granules. The programmed motion of the blade could be generated according to the rotational and vertical speeds applied by the blade, which corresponds to compression, slicing and lifting of the granules. Force versus distance curves corresponding to various cycles were recorded and the negative area under the “force versus distance” curves were estimated which is an indication of flow behavior.

Alumina dough prepared with 3 wt% of methyl cellulose corresponding to the CBVC region has been subjected to characterization for their rheological properties using an indigenously designed and fabricated extrusion rheometer described elsewhere [20]. The dough was then extruded at preset ram rates of 2, 10, 25,

50, and 75 mm/min, and the load versus displacement curves were recorded. Extrusion pressures, P , required for maintaining stable flow through the capillary die were calculated from the steady state load values corresponding to the plateau region of the load displacement curve, as load per unit cross sectional area of the barrel, $(4L/\pi \cdot D^2)$, where L is the load and D is the diameter of the barrel. Similarly, the extrusion velocities, V , corresponding to these pressures were calculated from the ram rates scaled for the relative change in the cross sectional area from the barrel to the capillary, as $v(D^2/d^2)$, where v is the ram rate and d is the diameter of the capillary die. For capillary extrusion through a round die, the shear stress and shear rate at the capillary wall can be calculated as per viscosity model. According to the viscosity model shear stress τ and shear rate $\dot{\gamma}$ can be calculated using $\tau = \Delta P/[4(L/d)]$, and $\dot{\gamma} = 8*(V/d)$, respectively, where ΔP -extrusion pressure, V -extrusion rate, L -die land length, D -diameter of the barrel and d -diameter of the capillary die. From the value of $\dot{\gamma}$ and τ , the viscosity can be calculated as $\eta = \tau / \dot{\gamma}$.

Alumina slurry prepared with powder was dispersed in water employing Darvan 821A (R. T. Vanderbilt Co., Inc., Norwalk, CT, USA) as a dispersant and 0.2 wt% MC as a binder. The slurry was milled in a pot jar mill using high purity alumina balls as the milling medium to obtain homogeneous slurry. Rheological behavior of the slurries was measured at varying shear rates using a controlled rheometer (MCR 51, Anton Paar, Austria) to determine the flow properties.

Fabrication of samples

Alumina mix corresponding to the sub-CBVC (granules) regime are shaped by compaction using a hydraulic press and CBVC regime (paste) were extruded using a ram type extruder. Further, the slurry corresponding to post CBVC region (slurry) was subjected to the slip casting. All the samples were dried at 110 °C and the green densities were estimated. The samples were machined to the rectangular specimens of 45 × 4 × 3 mm dimensions and flexural strength was evaluated using 3-point bend loading (ASTM C-1161-02C).

Thermal degradation studies

Thermal degradation of extruded samples with maximum 3.5 wt% methyl cellulose were subjected to thermogravimetric analysis. A Netzsch, TG/DTA analyzer that allows measurement of accurate weight loss as a function of temperature, in static air up to 800 °C was employed in the present study. TGA experiments are carried out at the heating rates of 5 °C/min, 10 °C/min, 20 °C/min and standard methods are employed for evaluating the kinetic parameters such as activation energy and pre-exponential factor. Weight loss can be regarded as the binder removal in progress with temperature

and hence

$$x = (m_o - m_T) / (m_o - m_f) \quad (1)$$

where, m_o -initial weight, m_T -sample weight at temperature T, m_f -final weight.

Arrhenius parameters, for the thermal decomposition of the samples were determined assuming a first order chemical reaction. This method uses the integral form of rate law. The rate law of any solid phase reaction is given as

$$\frac{dx}{dt} = A e^{(-E/RT)} f(x) \quad (2)$$

In non-isothermal TGA experiments, the heating rate is varied as a function of time and hence

$$\frac{dx}{dT} = \frac{dx}{dt} \times \frac{dt}{dT} \quad (3)$$

$$\frac{dx}{dT} = \frac{dx}{dt} \times \frac{1}{Y} \quad (4)$$

where Y is the heating rate given by dT/dt .

$$\frac{dx}{dT} = (A/Y) e^{(-E/RT)} f(x) \quad (5)$$

Plotting the left hand side of Eqn. 5 against the $1/T$ gives E/R as the slope and A as the intercept.

Sintering studies

Extruded samples were cut into cubes of 5 mm^3 and placed in a pushrod dilatometer (Netzsch, 402C Germany) and the shrinkage curve was recorded for all the three compacts as a function of temperature up to $1600 \text{ }^\circ\text{C}$ and time at constant heating rates of 5, 10 and $20 \text{ }^\circ\text{C}/\text{min}$. For non-isothermal sintering, the densification behavior can be generally expressed under a constant heating rate by :

$$d(\Delta L/L_o)/dt = K/(\Delta L/L_o)^n$$

where, $K = K_o \exp(-Q/RT)$ and $(\Delta L/L_o)$ stands for specimen shrinkage at any temperature. Young and

Cutler [21] estimated the sintering activation energy of oxides with success through an Arrhenius-type plot, i.e., $Td(\Delta L/L_o)/dt$ versus $1/T$, used a derivation by Johnson and Cutler [22] for intermediate-stage sintering. In principle, the plot of $Td(\Delta L/L_o)/dt$ versus $1/T$ yields a straight line with a slope of $-nQ/R$, where n is the characteristic of sintering mechanism, e.g. $n = 1/2$ for volume diffusion and $n = 1/3$ for grain-boundary diffusion, and Q is the activation energy for corresponding diffusion mechanism. The term nQ is representative of the effective activation energy of sintering. In addition to the kinetic analysis, densities of the sintered samples were also evaluated by Archimedes principle.

Results and Discussion

Characterization of the powder

The as-received alumina powder was subjected to XRD and SEM and results are shown in Fig. 1(a-b). The XRD pattern shows 100% alumina phase. SEM micrograph of the basic powder has shown an irregular morphology with an average particle size of 1 micron.

Binder volume concentration and processing regimes

Torque versus binder volume concentration curve recorded for alumina during CBVC measurements is shown in Fig. 2. It is evident that, initially when the amount of liquid media is very small, the liquid goes to replace the powder-air interface with powder-liquid interface, forming an adsorbed monolayer on the particles. As the liquid amount is increased, liquid bridging initiate amongst the individual particles, leading to the formation of particle clusters. As the powder mass undergoes shearing and mixing continuously, there exists a dynamic equilibrium, where the particle clusters are repeatedly broken down and formed again in a new particle packing arrangement in a cyclic fashion. The interparticle bonding occurs in the clusters due to the negative capillary pressure existing in the liquid bridge and the interfacial forces at the liquid-gas interface. Any disruption of the clusters during shearing has to overcome these forces along with the frictional forces due to mechanical interlocking of particles. Therefore, the mixing torque starts rising once particle clusters

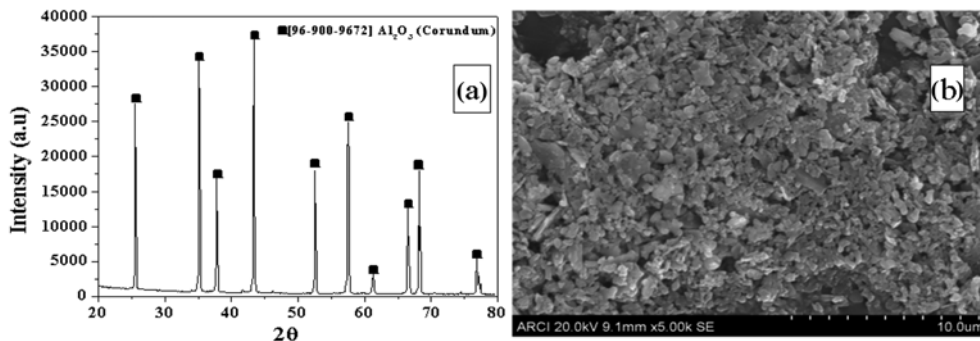


Fig. 1. (a) X-ray diffraction pattern and (b) Morphology of as received alumina powder.

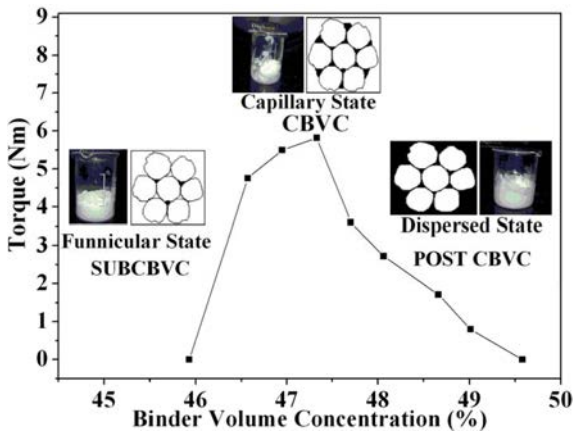


Fig. 2. Torque vs. binder volume concentration, showing the region of Sub-CBVC, CBVC and Post-CBVC.

begin to form, which is a measure of the extent of resistance offered by the clusters to deform in a shear field. Once the point of CBVC is crossed, the particle structure gets dilated and reduces inter-particle friction and thereby freeing the entrapped liquid. The mean particle distance increases and the mix are akin to a dispersion of solid particles in a liquid medium. But bigger clusters form by the growth of smaller ones as more and more liquid is added, until the mass becomes a coherent paste at the point of CBVC, which is the capillary state. The mixing torque then becomes

primarily the viscosity of the liquid medium as altered by the presence of the powder particles and it falls off as the binder content is increased. As the amount of the liquid is further increased, the liquid is entirely filled in the voids.

Flow behavior of regimes

Sub CBVC regime

SEM micrographs showing morphology of granules along with the force versus distance curves for granules are shown in Fig. 3(a-b). Based on these curves recorded, cohesion index (the ratio of cohesion coefficient and sample weight) is calculated by integrating the negative areas under the curve. The cohesion index of the granules was found to be around 11, indicating a free flowing behavior.

CBVC regime

Fig. 4(a) shows a plot of the variation of viscosity versus shear rate. The viscosity tends to decrease with the shear rate, suggesting a shear thinning behaviour of the dough. Such a non-Newtonian flow behaviour has been analyzed using the Power Law Model, $\eta = m * \dot{\gamma}^{n-1}$, where η -viscosity, m -consistency constant, $\dot{\gamma}$ -shear rate and n -shear rate exponent or power law index, proposed by Ostwald de Wale for the pseudo plastic polymeric materials. Figure 4(b) shows a plot of $\ln \eta$ vs. $\ln \dot{\gamma}$ plot for the alumina dough. The power law

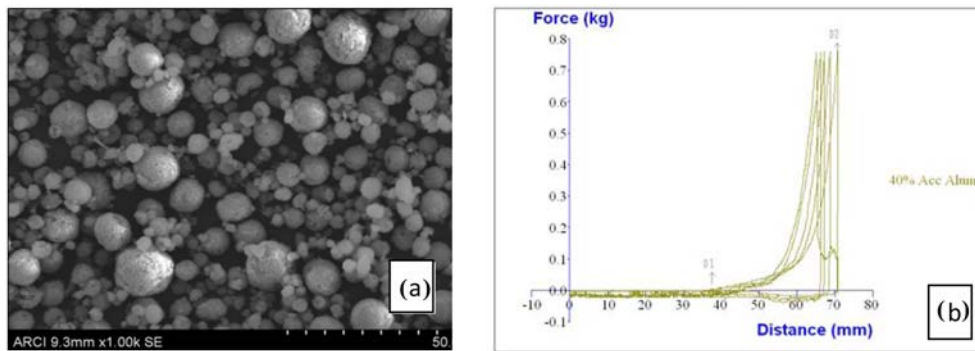


Fig. 3. (a) Morphology of the spray dried powder and (b) Force versus distance curves (Cohesion index measurement).

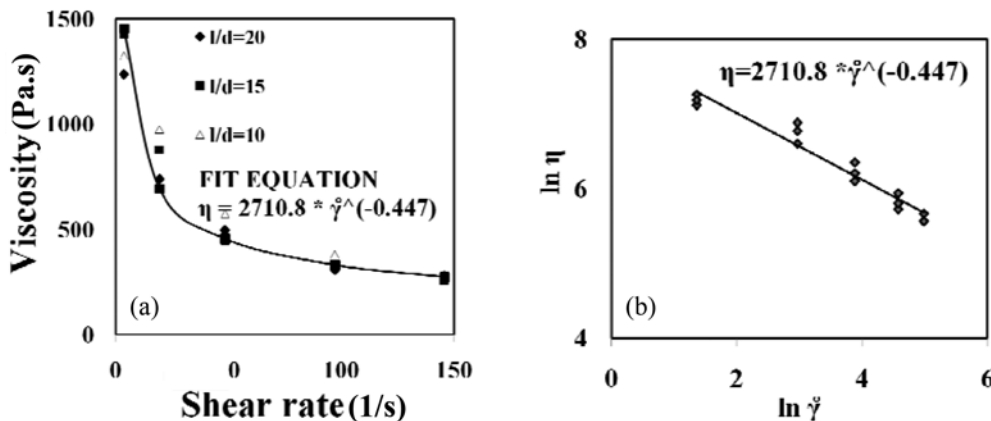


Fig. 4. (a) Variation of the viscosity as a function of the shear rate and (b) $\ln \eta$ vs. $\ln \dot{\gamma}$ plot for the alumina dough.

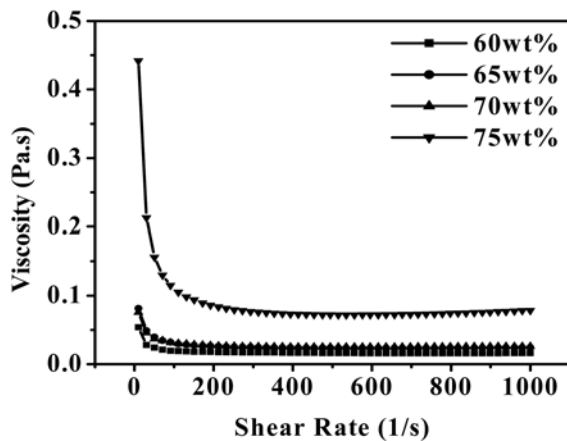


Fig. 5. Viscosity versus shear rate of alumina slurries with varying solid loadings.

Table 1. Green densities of alumina samples processed through various techniques.

Sr. No.	Processing	Green density ($\text{g}\cdot\text{cm}^{-3}$)	% TD
1	Compaction	2.01	50.42
2	Extrusion	1.78	44.65
3	Slip casting	1.86	46.66

model is applicable in the present study as the graph of $\ln \eta$ vs. $\ln \dot{\gamma}$ is linear. At various shear rates, the mix shows a shear rate exponent of 0.55, indicating the pseudo plastic behavior.

Post CBVC regimes

Fig. 5 shows the viscosity measurements with shear rates of alumina slurries with varying solid loading. Electrostatic stabilization and hence interaction between the particles is evident from the viscosity versus shear rate plot. It is evident that the slurry exhibits a pseudo plastic behavior at lower shear rates and as the shear rate is increased beyond 250s^{-1} , the slurry exhibited close to Newtonian behavior. This behavior indicates the suitability of casting process optimized through electrostatic stabilization with the dispersant to a maximum solid loading of 70 wt%.

Green density and flexural strength measurement of green specimens

Green density of the Sub CBVC (compacted), CBVC (extruded) and Post CBVC (slip cast) samples were estimated by dimensional method and are shown in Table 1. Compaction processing exhibited the maximum density of $2.01\text{ g}\cdot\text{cm}^{-3}$, corresponding to a maximum of 50% of TD due to particle interlocking.

Fig. 6(a-c) show the plots of the flexural strength versus binder content for Sub CBVC (compacted), CBVC (extruded) and Post CBVC (slip cast) rectangular bars. It clearly indicates that the flexural strength of the samples is maximum at the percentage

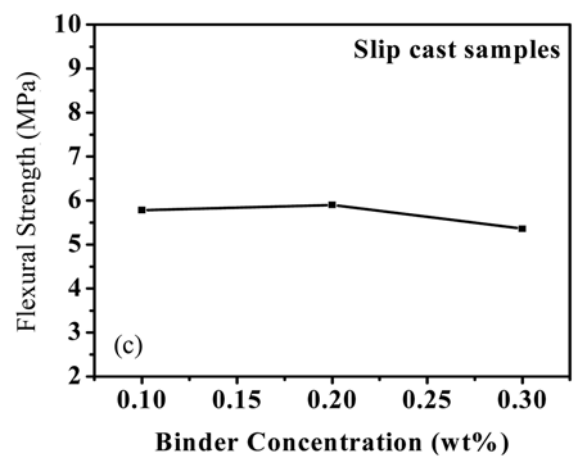
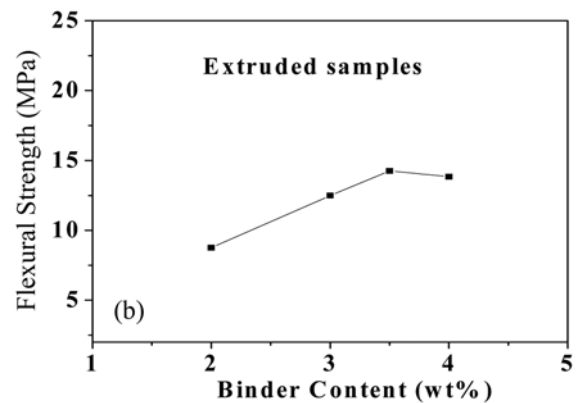
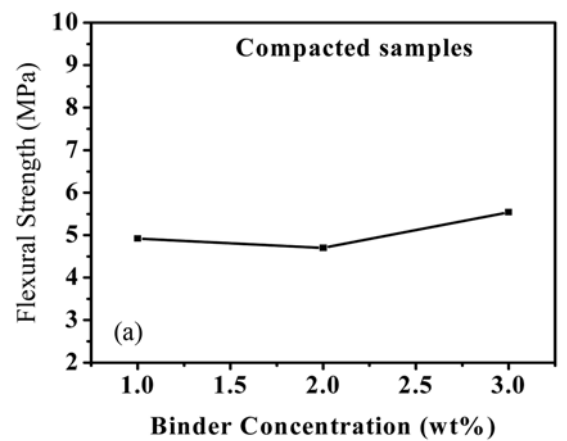


Fig. 6. Plots of the flexural strength vs. the binder content of samples processed through (a) compaction (b) Extrusion and (c) Slip cast processes.

of binder at around 1 wt% and remains relatively constant till 2 wt% with a marginal increase till 3 wt% in case of compacted samples. In case of slip cast samples, strength is maximum in the range of 0.1-0.2 wt% followed by a decrease at around 0.3 wt%. Dough corresponding to CBVC exhibited a maximum strength at 3-4 wt% of the binder content. It is evident that green strengths of the samples have exhibited a correlation with the binder content and is high in the case of extruded samples.

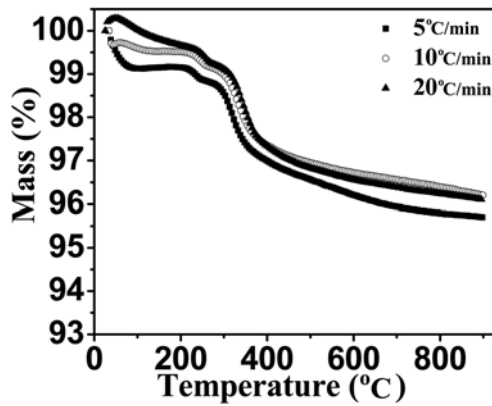


Fig. 7. TGA (Weight loss vs. temperature) of Methyl Cellulose (3, 5, 10 and 20 °C/min).

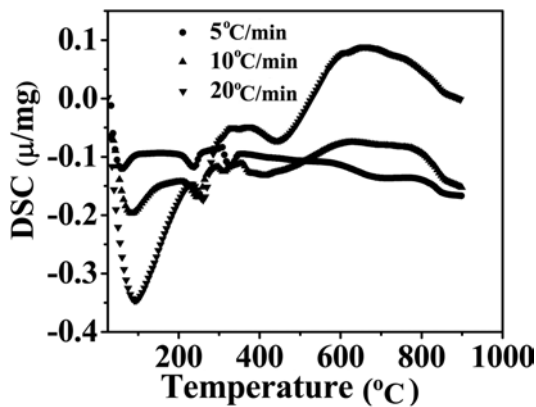


Fig. 8. DSC (Weight loss vs. temperature) of Methyl Cellulose (3, 5, 10 and 20 °C/min).

Binder burn out and kinetics of methyl cellulose pyrolysis

TG-DSC curves recorded are shown in Fig. 7&8. During ceramic processing generally the binders are removed by thermolysis in an oxidizing atmosphere. It is evident from the TG curve that when the samples exposed to a ramp rate of 5 °C/min, methyl cellulose start losing weight at around 180 °C and continues to lose weight with relatively sharp transitions around 240 °C and 350 °C. DSC plots also complements with strong endothermic and a weak exothermic peak in these temperature regimes. On increasing ramp rates beyond 10 °C/min, the pattern has shown an additional peak at around 440 °C, suggesting a different mechanism for the binder removal. Thermal scission of methyl cellulose is generally occurs through the pyrolysis reactions such as primary thermal decomposition followed by the secondary thermal decomposition reactions. Chemical species of primary thermal decomposition resulting from de-polymerization or fragmentation may not be volatile might undergo condensation or polymerization to form the char.

The data obtained from TGA studies shown in Fig. 9(a) for the heating rates of 5 °C/min, 10 °C/min and 20 °C/min are used for the kinetic calculations. Extent

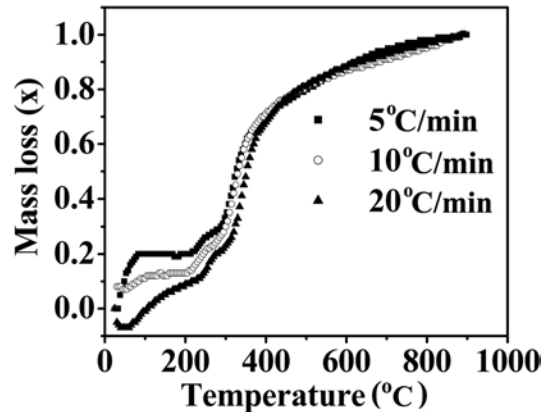


Fig. 9(a). Plot of mass loss versus temperature.

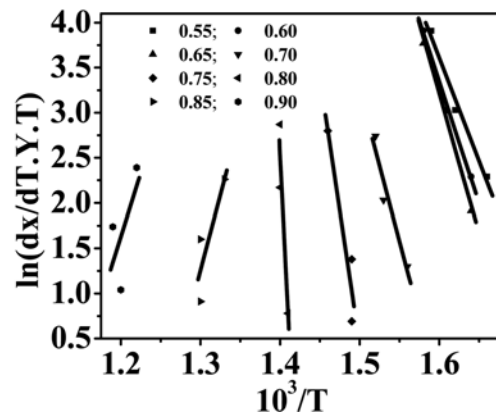


Fig. 9(b). Plot of $\ln[(dx/dT).Y.T]$ versus $1/T$ gives the Arrhenius parameters A (pre-exponential factor) and E (activation energy) for MC.

of thermal decomposition $\ln[(dx/dT).Y.T]$ vs. $1/T$ is calculated as per the standard kinetics calculation depicted vide equations (1) to (5) and the corresponding plot is shown in Fig. 9(b). The plot exhibits a straight line obtained by linear regression. The slope of the straight line gives E/R and the activation energy is estimated to be around 75-110 kJ/mole.

Kinetics of Sintering

Fig. 10(a) gives the relation between density and temperature for different heating rates of fine alumina green bodies sintered to 1600 °C. It can be noted that the sintered densities obtained at any temperature showed a modest, but a systematic dependence on heating rates. The variation in density with sintering temperature followed a similar trajectory regardless of the heating rate. Fig. 10(b) shows the densification rate versus temperature plot for the three different heating rates. The instantaneous densification rate increases from green state to the intermediate stage of sintering, undergoes a maximum and then decreases with increasing density. The maximum of the curves shifts slightly to higher temperature with increasing heating rate.

Master Sintering Curve (MSC) constructed from densification data displayed in Fig. 10(a) is shown in

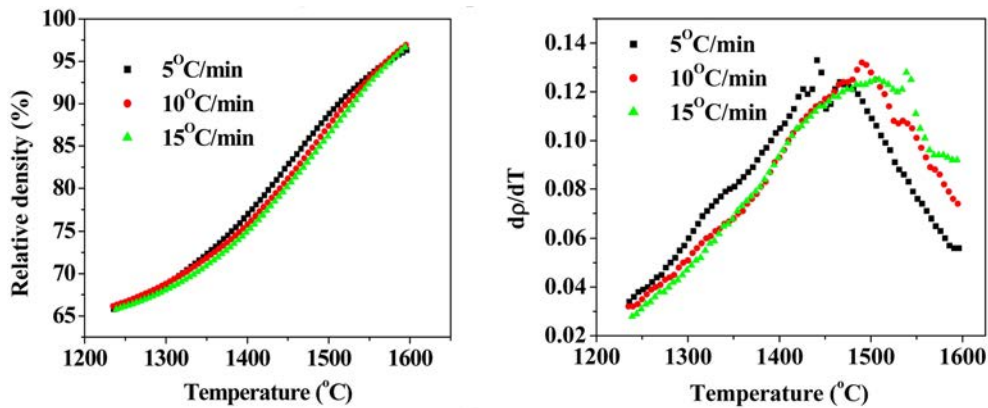


Fig. 10. (a-b) Relative densities and densification rate versus temperature profiles of the compacts at different heating rates of 5, 10 and 15 °C/min.

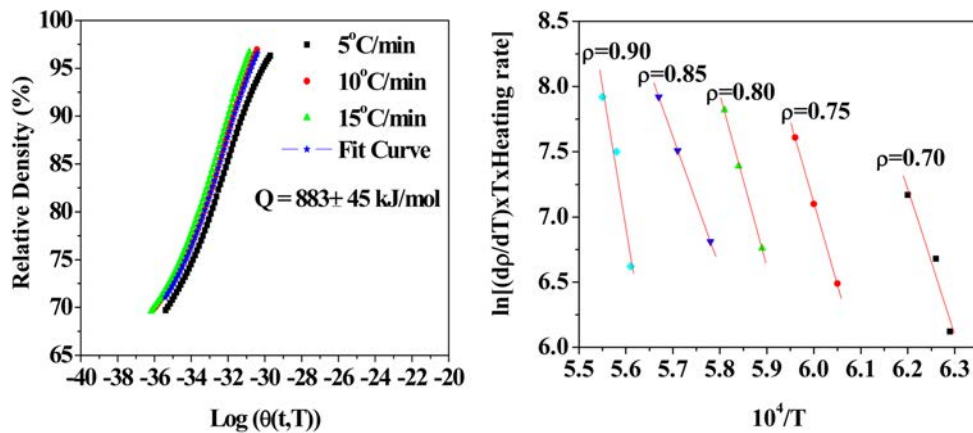


Fig. 11. (a-b) MSC for constant heating rate of Alumina compacts and Arrhenius plot of $\ln(dp/dt \times T \times \text{Heating rate})$ vs. $1/T$ for the non-isothermal sintering of the powder compacts at different heating rates corresponding to the same relative density.

Table 2. Physical properties of alumina sintered samples.

Sr. No.	Processing	Sintered density ($\text{g}\cdot\text{cm}^{-3}$)	% TD	Apparent porosity (%)	Water absorption (%)
1	Compaction	3.96	99.33	0.07	0.017
2	Extrusion	3.94	98.83	0.20	0.050
3	Slip casting	3.97	99.58	0.05	0.012

Fig. 11(a). The value of $\theta(t, T)$ changed dramatically from 10-36 (at the beginning) to 10-29 at the high-density end (~97%). Despite the change in heating rates, the individual sintering curves appear to be close to each other. This indicates that there must have a general curve, regardless of the sintering path, which is what we have defined as the Master Sintering Curve.

The activation energy of sintering is essentially able to be evaluated by an Arrhenius plots of $\ln(dp/dt \times T \times \text{Heating rate})$ versus the reciprocal of the absolute temperature for the samples sintered isothermally or non-isothermally as shown in Fig. 11(b). It is clear that the straight lines obtained are not parallel. Similar phenomena can be found in the literature [23]. According to the slope of the straight lines, the different apparent values for Q ranging from 928 kJ/mol (0.7 of relative density) to 838 kJ/mol (0.85 of relative density) can be

obtained. The activation energy for densification is evaluated as 883 ± 45 kJ/mol for the slopes of the linear representation. The activation energy for densification of the fine-grained ceramics is close to that measured by Fang et al (2003) i.e., 1080 kJ/mol, when the lattice diffusion is the dominant mechanism [24].

The samples processed through extrusion processing along with the other techniques are subjected to sintering at 1600 °C in air sintering furnace. Sintered densities of the samples are characterized by Archimedes principle and are presented in Table 2. Though there is a significant variation in green densities, final sintered densities were in the range of 98-99.5%.

Conclusions

Torque rheometric study of alumina distinctly identifies

three processing regimes with respect to binder volume concentrations corresponding to compaction, extrusion and slip casting. Compacted samples exhibited high green densities in comparison to the extruded samples, which can be attributed to the high compaction pressure leading to particle inter-locking in the process. However, the green strength of the samples is found to be a strong function of the binder content. A cohesion index of 11 for granules were found suitable for compaction and a shear thinning behavior corresponding to shear rate exponent less than 1 are found suitable for extrusion and slip casting. Binder burn out kinetic studies estimated an activation energy of 75-110 kJ/mol. Kinetic analysis of sintering through constructing the Master Sintering Curves (MSC) estimated an activation energy of 883 ± 45 kJ/mol. Final density of the samples is found to be in the range of 98-99.5% of the TD irrespective of the green densities and binder content under optimized processing conditions.

Acknowledgments

The authors like to thank Dr. M. Vijay Kumar, Scientist for extending their experimental facilities at DMRL.

References

1. M.N. Rahaman, Ceramic Processing and Sintering, Marcel Dekker, New York (1995) 1.
2. F.F. Lange, Powder processing science and technology for increased reliability. *J. Am. Ceram. Soc.* 72 (1989) 3-10.
3. T. A. Ring, Fundamentals of Ceramic Powder Processing and Synthesis, Chapter 15, Academic Press Inc., San Diego (1996) 729.
4. J.S. Reed, Principles of Ceramics Processing, 2nd edition, John Wiley & Sons, Inc., New York (1995) 1.
5. G.Y. Onoda, Jr., in Ceramic Processing Before Firing (G. Y. Onoda, Jr and L.L. Hench, Eds.) Wiley, New York (1978) 235.
6. B.V. Velamakanni, F. F. Lange, F. W. Zok, and D. S. Pearson, Influence of Interparticle Forces on the Rheological Behavior of Pressure-Consolidated Alumina Particle Slurries, *J. Am. Ceram. Soc.* 77 (1994) 216-220.
7. Y. K. Leong, Exploitation of interparticle forces in the processing of colloidal ceramic materials, *Mat. & Des.* 15 (1994) 141.
8. A.M. Hollenbach, M. Peleg, R. Rufner, Interparticle surface affinity and the bulk properties of conditioned powders, *Powder Technology* 35 (1983) 51-62.
9. M. Subbanna, P.C. Kapur, Pradip, Role of powder size, packing, solid loading and dispersion in colloidal processing of ceramics, *Ceram. Inter.* 28 (2002) 401-405.
10. J. A. Lewis, Binder Removal from Ceramics, *Annu. Rev. Mater. Sci.* 27 (1997) 147-73.
11. R. V. Shende and S. J. Lombardo, Determination of Binder Decomposition Kinetics for Specifying Heating Parameters in Binder Burnout Cycles, *J. Am. Ceram. Soc.* 81 [4] (1998) 1053-1057.
12. S. Masia, P. D. Calvert, W. E. Rhine, and H. K. Bowen, Effects of Oxides on Binder Burnout During Ceramics Processing, *J. Mater. Sci.* 24 [6] (1989) 1907-1912.
13. J. Daniel. Shanefield, Organic Additives and Ceramic Processing, Kluwer Academic Publishers, Dordrecht (1995) 1.
14. Anirban Das, Giridhar Madras, Niladri Dasgupta, Arun M. Umarji, Binder removal studies in ceramic thick shapes made by laminated object manufacturing, *J. Eur. Ceram. Soc.* 23 (2003) 1013-1017.
15. T. Chartier, M. Ferrato, J.F. Baumard, Supercritical debinding of injection molded ceramics. *J. Am. Ceram. Soc.* 78 (1995) 1787-1792.
16. M.J. Cima, J.A. Lewis and A.D. Devoe, Binder distribution in ceramic green ware during thermolysis, *J. Am. Ceram. Soc.* 72 [7] (1989) 1192-1198.
17. H. M. Shaw, M. J. Edirisinghe and S. Holding, Binder degradation and redistribution during pyrolysis of ceramic injection mouldings, *J. Mater. Sci. Lett.* 12 [15] (1993) 1227-1230.
18. Kazuto Kobayashi, Ching-i Huang, Timothy P. Lodge, Thermoreversible Gelation of Aqueous Methylcellulose Solutions, *Macromolecules* 32 (1999) 7070-7077.
19. M.D. Ashton, R. Farely, F.H.H. Valentin, Some investigations into the strength and flow properties of powders. *Rheologica Acta* 4 [3] (1965) 206-218.
20. M. Swathi, R. Papitha, U. S. Hareesh, B. P. Saha and R. Johnson, Rheological Studies on Aqueous Alumina Extrusion Mixes, *Transactions of the Indian Institute of Metals* 64 [6] (2011) 541-547.
21. Wayne S. Young, Ivan B. Cutler, Initial Sintering with Constant Rates of Heating, *J. Am. Ceram. Soc.* 53 [12] (1970) 659-663.
22. D. Lynn Johnson, Ivan B. Cutler, Diffusion Sintering: II, Initial Sintering Kinetics of Alumina, *J. Am. Ceram. Soc.* 46 [11] (1963) 545-550.
23. Z.Y. Liu, N.H.Loh, K.A.Khor and S.B.Tor, Sintering activation energy of powder injection molded 316L stainless steel, *Scripta Materialia* 44 (2001) 1131-1137.
24. Tsang-Tse Fang, Jyh-Tzong Shiue, Fuh-Shan Shiau, On the evaluation of the activation energy of sintering, *Mater. Chem. & Phys.* 80 [1] (2003) 108-113.